

EXPERIENCES WITH NEGATIVE NORM LEAST-SQUARE METHODS FOR THE NAVIER-STOKES EQUATIONS*

P. BOCHEV†

Abstract. This paper is concerned with the implementation and numerical study of a discrete negative norm least-squares method for the Navier-Stokes equations proposed in [2] and [3]. The main focus of the paper is on the algorithmic development and computational analysis of this method, including design of efficient preconditioners, numerical estimates of convergence rates, etc. Our experiments indicate that the negative norm method yields results that are in agreement with the theoretical error estimates of [3] and compare favorably with the benchmark studies of [11].

Key words. Navier-Stokes equations, least-squares principle, finite element methods.

AMS subject classifications. 76D05, 76D07, 65F10, 65F30.

1. Introduction. In this paper we examine algorithmic and computational issues related to a negative norm least-squares method for the numerical solution of the stationary, incompressible Navier-Stokes equations. In the recent years methods of least-squares type for fluid flow problems have been receiving increasing attention; see e.g., [1]-[9], [15], [16], [17], and [18] among others. This interest is largely caused by the attractive analytic and computational features of least-squares methods that are not present in other discretization schemes, such as mixed Galerkin methods. Most of these features stem from the fact that weak variational problems in least-squares methods represent necessary minimum conditions for problem-dependent functionals which are defined by summing up residual norms of the differential equations. The guiding principle in the choice of the norms is to obtain *norm-equivalent* functionals. Then, corresponding weak problems are in general coercive and their discretization leads to symmetric and positive definite algebraic systems. Specifically, in the context of the Navier-Stokes equations application of least-squares variational principles offers the following advantages:

- methods are not subject to the inf-sup (LBB) stability condition; see [12] and [14];
- used in conjunction with Newton linearization least-squares lead to symmetric, positive definite linear systems, at least in a neighborhood of the solution;
- essential boundary conditions can be enforced in a weak, variational sense.

As a result,

- a single approximating space can be used for both the velocity and the pressure leading to simplified and more efficient algorithmic design;
- solution of the linearized problems can be accomplished by robust and efficient iterative methods without assembling the discretization matrix;
- approximating spaces are not subject to the essential boundary conditions.

However, without a thorough examination of the settings for the least-squares method many of these advantages may be lost or utilized incompletely. For example, a least-squares method based on the primitive variable Navier-Stokes equations may require conforming discretizations by continuously differentiable finite element spaces, i.e., it will be impractical. Furthermore, if the least-squares functional is not norm-equivalent then resulting methods may fail to be optimally accurate.

*Received May 14, 1997. Accepted for publication August 29, 1997. Communicated by S. Parter.

†Department of Mathematics, Box 19408, University of Texas at Arlington, Arlington, TX 76019-0408, (bochev@utamat.uta.edu). This work was sponsored by the National Science Foundation under grant number DMS-9705793.

In this paper we consider a method, developed and analyzed in [2]-[3], that combines decomposition of the Navier-Stokes equations into a first-order system with the use of negative Sobolev space norms in the least-squares functional. The first feature allows us to define a method that can be implemented using standard finite element spaces. Indeed, most of the recent research in least-squares methods has focused on settings that involve such decompositions; see, e.g., [1], [2], [3], [4], [16], and [17]. The second feature leads to a norm equivalent functional that is meaningful for less regular solutions than an L^2 -functional associated with the same system. The use of negative norms to measure equation residuals has been, perhaps, first considered by Glowinski et al. in [13]. However, the method of [13] casts the Navier-Stokes problem into the framework of an optimal control problem, whereas here we consider a bona-fide least-squares minimization principle. In that context the first use of negative norms is due to Bramble et al. [7].

In the next section we introduce the relevant notation. Then in §2 we state the first-order *velocity-flux* Navier-Stokes system that will be used to define the least-squares method. The method and a necessarily brief account of the theoretical results established in [2]-[3] are presented in §3. The core of the paper is contained in §§4-5. Section 4 discusses implementation of the negative norm method, while in §5 we present computational study of this method and compare it with two other L^2 least-squares methods for the velocity-flux Navier-Stokes equations.

1.1. Notation. In what follows Ω will denote an open, bounded region in \mathbf{R}^2 having a Lipschitz continuous boundary. Throughout the paper vectors will be denoted by bold face letters, e.g., \mathbf{u} and tensors by underlined bold face capitals, e.g., $\underline{\mathbf{U}}$. In what follows ∇ will denote the gradient operator and ∇^t the divergence operator. For tensor variables $\nabla^t \underline{\mathbf{U}}$ will denote a vector whose components are the divergencies of the corresponding columns in $\underline{\mathbf{U}}$. With C we denote a positive constant whose meaning and value changes with context. We recall the standard Sobolev spaces $H^s(\Omega)$ with corresponding inner products denoted by $(\cdot, \cdot)_{s,\Omega}$ and norms by $\|\cdot\|_{s,\Omega}$. Sobolev spaces for vectors and tensors will be denoted by $\mathbf{H}^s(\Omega)$ and $\underline{\mathbf{H}}^s(\Omega)$, respectively. Often we will use the space $H_0^1(\Omega)$ consisting of all $H^1(\Omega)$ functions that vanish on the boundary and the space $L_0^2(\Omega)$ consisting of all square integrable functions with zero mean with respect to Ω . The dual of $H_0^1(\Omega)$ will be denoted by $H^{-1}(\Omega)$. For this space we introduce the following norm

$$(1.1) \quad |\phi|_{-1} = \sup_{\psi \in H_0^1(\Omega)} \frac{(\phi, \psi)}{|\psi|_1},$$

where

$$|\psi|_1 = \|\nabla \psi\|_0$$

is the usual seminorm on $H^1(\Omega)$.

We let \mathcal{T}_h denote a regular triangulation of the domain Ω into finite elements. The parameter h is associated with the size of the finite elements, which can be either triangles or rectangles. For finite element spaces defined on triangles we use the standard notation P_k , i.e., P_k is the space of all continuous, over Ω , piecewise polynomial functions u^h such that in each triangle u^h is a polynomial of degree k . Similarly, Q_k will be used to denote finite element spaces defined with respect to a triangulation of Ω into rectangles. In that case, on each rectangle u^h is a polynomial function whose degree in each coordinate direction does not exceed k .

We recall that the spaces P_k and Q_k have the following property, see, e.g., [10], for $k \geq 1$, given a function $u \in H^{k+1}(\Omega)$, there exists an element w^h in P_k (or Q_k) such that

$$(1.2) \quad \|u - w^h\|_r \leq Ch^{k+1-r} \|u\|_{k+1}, \quad r = 0, 1,$$

where the constant C is independent of h .

2. The first-order system. We consider the steady state incompressible Navier-Stokes equations given by

$$(2.1) \quad -\nu \Delta \mathbf{u} + (\nabla \mathbf{u}^t)^t \mathbf{u} + \nabla p = \mathbf{f} \quad \text{in } \Omega$$

$$(2.2) \quad \nabla^t \mathbf{u} = \mathbf{0} \quad \text{in } \Omega,$$

along with the velocity boundary condition

$$(2.3) \quad \mathbf{u} = \mathbf{0} \quad \text{on } \Gamma .$$

In (2.1)-(2.2) \mathbf{u} , p and \mathbf{f} denote velocity, pressure and given body force, respectively, and ν is the inverse of the Reynolds number. The system (2.1)-(2.2) is customarily considered with the zero-mean pressure constraint given by

$$(2.4) \quad \int_{\Omega} p d\Omega = 0.$$

To effect the first-order transformation of (2.1)-(2.2) we introduce the velocity flux variable

$$(2.5) \quad \underline{\mathbf{U}} = \nabla \mathbf{u}^t ,$$

which is a tensor with entries $U_{ij} = \partial u_j / \partial x_i$, $1 \leq i, j \leq n$. Then,

$$(\nabla^t \underline{\mathbf{U}})^t = \Delta \mathbf{u}$$

and

$$(\nabla \mathbf{u}^t)^t \mathbf{u} = \underline{\mathbf{U}}^t \mathbf{u} .$$

As a result, the Navier-Stokes equations (2.1)-(2.2) can be replaced by the first-order system

$$(2.6) \quad -(\nabla^t \underline{\mathbf{U}})^t + \lambda \underline{\mathbf{U}}^t \mathbf{u} + \nabla p = \mathbf{f} \quad \text{in } \Omega$$

$$(2.7) \quad \nabla^t \mathbf{u} = \mathbf{0} \quad \text{in } \Omega$$

$$(2.8) \quad \underline{\mathbf{U}} - \nabla \mathbf{u}^t = \underline{\mathbf{0}} \quad \text{in } \Omega,$$

along with (2.3) and (2.4). In the new system, momentum equation (2.6) is weighted by $\lambda = 1/\nu$ which is convenient for the analysis; see [3]. For simplicity, rescaled pressure and body force are denoted again by the same symbols. In view of (2.5) and (2.2) the system (2.6)-(2.8) can be augmented by two additional equations and a boundary condition, given by

$$(2.9) \quad \nabla(\text{tr} \underline{\mathbf{U}}) = \mathbf{0} \quad \text{in } \Omega,$$

$$(2.10) \quad \nabla \times \underline{\mathbf{U}} = \underline{\mathbf{0}} \quad \text{in } \Omega,$$

and

$$(2.11) \quad \mathbf{n} \times \underline{\mathbf{U}} = \underline{\mathbf{0}} \quad \text{on } \Gamma ,$$

respectively.

3. Negative norm least-squares methods. In this section we outline the least-squares method developed in [2]-[3] and state the error estimates established in [3]. We recall that the choice of least-squares functionals is guided by two main objectives. First, the resulting method should be practical in the sense that it can be implemented using standard finite element spaces such as P_k and Q_k . Second, the method should be optimal in the sense that approximations converge at the rate of the best approximation out of the finite element space, provided the exact solution is smooth enough.

The first objective can be easily met by using first-order systems to define least-squares functionals. Indeed, since equations (2.6)-(2.8) involve only first-order derivatives, the functional

$$(3.1) \quad J(\underline{\mathbf{U}}, \mathbf{u}, p) = \| -(\nabla^t \underline{\mathbf{U}})^t + \lambda \underline{\mathbf{U}}^t \mathbf{u} - \mathbf{f} + \nabla p \|_0^2 + \|\nabla^t \mathbf{u}\|_0^2 + \|\underline{\mathbf{U}} - \nabla \mathbf{u}^t\|_0^2,$$

defined by summing up the L^2 -norms of equation residuals leads to a practical method. However, the second objective requires the least-squares functional to be norm equivalent. To define such a functional one first has to determine function spaces for the data and the solution $U = (\underline{\mathbf{U}}, \mathbf{u}, p)$ in which the Stokes problem, associated with (2.6)-(2.8) is well-posed. Then, each equation residual in (2.6)-(2.8) has to be measured in the corresponding data space norm. This guarantees that the functional with zero data and a linearized convective term will be equivalent to a norm on the solution space, provided that the Navier-Stokes equations have a nonsingular solution; see [2]. In particular, we have that (see [9]) the first-order Stokes problem is well-posed in the spaces

$$(3.2) \quad \mathbf{X} = \tilde{\mathbf{L}}^2(\Omega) \times \mathbf{H}_0^1(\Omega) \times L_0^2(\Omega)$$

and

$$(3.3) \quad \mathbf{Y} = \mathbf{H}^{-1}(\Omega) \times L^2(\Omega) \times \tilde{\mathbf{L}}^2(\Omega),$$

for the solution and the data, respectively, and that the a priori estimate relevant to the least-squares method is given by

$$(3.4) \quad \|\underline{\mathbf{U}}\|_0 + \|\mathbf{u}\|_1 + \|p\|_0 \leq C \left(| -(\nabla^t \underline{\mathbf{U}})^t + \nabla p |_{-1} + \|\nabla^t \mathbf{u}\|_0 + \|\underline{\mathbf{U}} - \nabla \mathbf{u}^t\|_0 \right).$$

As a result, a norm equivalent functional for (2.6)-(2.8) is given by

$$(3.5) \quad J(\underline{\mathbf{U}}, \mathbf{u}, p) = | -(\nabla^t \underline{\mathbf{U}})^t + \nabla p + \lambda \underline{\mathbf{U}}^t \mathbf{u} - \mathbf{f} |_{-1}^2 + \|\nabla^t \mathbf{u}\|_0^2 + \|\underline{\mathbf{U}} - \nabla \mathbf{u}^t\|_0^2.$$

Estimate (3.4) also indicates that functional (3.1) is not coercive in the norm in which it is continuous, i.e., it is not equivalent to a norm on a product of H^1 spaces. In [9] it has been shown that an L^2 -functional that is H^1 -norm equivalent can be defined using the augmented velocity flux system (2.6)-(2.8), and (2.9)-(2.11):

$$(3.6) \quad J(\underline{\mathbf{U}}, \mathbf{u}, p) = \| -(\nabla^t \underline{\mathbf{U}})^t + \lambda \underline{\mathbf{U}}^t \mathbf{u} - \mathbf{f} + \nabla p \|_0^2 + \|\nabla^t \mathbf{u}\|_0^2 + \|\underline{\mathbf{U}} - \nabla \mathbf{u}^t\|_0^2 + \|\nabla(\text{tr} \underline{\mathbf{U}})\|_0^2 + \|\nabla \times \underline{\mathbf{U}}\|_0^2.$$

Analysis of finite element methods based on (3.6) can be found in [2]. Although the focus of this paper is on a different type of least-squares functionals we shall use (3.1) and (3.6) in §5 to compare and contrast performance of various least-squares methods.

A necessary condition for minimization of (3.5) over the space \mathbf{X} is given by the following nonlinear variational problem:

seek $(\underline{\mathbf{U}}, \mathbf{u}, p) \in \mathbf{X}$ such that

$$\begin{aligned}
 & \mathcal{B}((\underline{\mathbf{U}}, \mathbf{u}, p), (\underline{\mathbf{V}}, \mathbf{v}, q)) \\
 & \equiv (-\nabla^t \underline{\mathbf{U}})^t + \nabla p + \lambda \underline{\mathbf{U}}^t \mathbf{u} - \mathbf{f}, -(\nabla^t \underline{\mathbf{V}})^t + \lambda (\underline{\mathbf{U}}^t \mathbf{v} + \underline{\mathbf{V}}^t \mathbf{u}) + \nabla q)_{-1} \\
 (3.7) \quad & + (\nabla^t \mathbf{u}, \nabla^t \mathbf{v})_0 + (\underline{\mathbf{U}} - \nabla \mathbf{u}^t, \underline{\mathbf{V}} - \nabla \mathbf{v}^t)_0 = 0
 \end{aligned}$$

for all $(\underline{\mathbf{V}}, \mathbf{v}, q) \in \mathbf{X}$.

Formally, one can define a least-squares method based on (3.5) by choosing a finite element subspace \mathbf{X}^h of \mathbf{X} and restricting the variational problem (3.7) to \mathbf{X}^h ; see [2]. Such a method is, however, only of theoretical interest. Indeed, because the negative norm is not computable, forming the algebraic problem that corresponds to a discretization of (3.7) over the space \mathbf{X}^h is not feasible. In the next section we introduce a discrete negative norm counterpart of (3.5) which results in a practical least-squares method.

3.1. The discrete negative norm method. To define the discrete negative norm we follow an approach similar to the one suggested by Bramble et al. in [7]. Consider the Dirichlet problem

$$(3.8) \quad -\Delta u = f \quad \text{in } \Omega, \quad u = 0 \quad \text{on } \Gamma.$$

Let $X^h \subset H^1(\Omega)$ denote a finite element space and let S^h denote a finite element solution operator for (3.8), i.e.,

$S^h f = u_h \in X^h \cap H_0^1(\Omega)$ for $f \in H^{-1}(\Omega)$ if and only if u_h solves the problem: seek $u_h \in X^h \cap H_0^1(\Omega)$ such that

$$(3.9) \quad \int_{\Omega} \nabla u_h \cdot \nabla v_h dx = \int_{\Omega} f v_h dx, \quad \forall v_h \in X^h \cap H_0^1(\Omega).$$

It can be shown (see [7]) that

$$(3.10) \quad (S^h f, f) = \sup_{\phi_h \in X^h \cap H_0^1(\Omega)} \frac{(f, \phi_h)^2}{|\phi_h|_1^2}.$$

Since the right hand side in (3.10) is restriction of (1.1) to X^h , it follows that

$$(3.11) \quad |f|_{-1,h}^2 = (S^h f, f), \quad \forall f \in H^{-1}(\Omega).$$

defines a computable semi-norm on $H^{-1}(\Omega)$, associated with a semi-definite inner product given by $(f, g)_{-1,h} = (S^h f, g)_0 = (f, S^h g)_0$. However, the cost of computing S^h may still be prohibitive. Thus, following [7], S^h is further replaced by a symmetric and positive semidefinite operator B^h , defined on L^2 . This operator is assumed to be spectrally equivalent to S^h in the sense that

$$(3.12) \quad C_0(S^h \phi, \phi)_0 \leq (B^h \phi, \phi)_0 \leq C_1(S^h \phi, \phi)_0.$$

The main consideration in the choice of B^h is computational cost. The cost of computing $B^h \phi$ must be significantly lower than the cost of computing $S^h \phi$. Once B^h is chosen it is easy to see that

$$(3.13) \quad |f|_{-h}^2 = (B^h f, f)$$

defines a computable *semi-norm*, equivalent to (3.11). Then, a computable discrete negative *norm* can be defined (see [7]) by adding to (3.13) an L^2 -term weighted by h^2 :

$$(3.14) \quad \|\phi\|_{-h}^2 = (\widetilde{S}^h \phi, \phi)_0, \quad \text{where} \quad \widetilde{S}^h = \alpha h^2 I + B^h.$$

The inner product associated with (3.14) is given by

$$(3.15) \quad (\phi, \xi)_{-h} = (\widetilde{S}^h \phi, \xi)_0.$$

Norm (3.14) is equivalent to (1.1) in the sense that

$$(3.16) \quad \frac{1}{C} |u|_{-1} \leq \|u\|_{-h} \leq C (h \|u\|_0 + |u|_{-1})$$

for all $u \in L^2(\Omega)$. Without the term $h^2 I$, the lower bound in (3.16) does not hold, i.e., this equivalence relation is not valid for the *semi-norm* (3.13). The additional weight α can be used to tune up the performance of the method and its choice will be discussed later.

Using (3.14) we introduce the following counterpart of (3.5):

$$(3.17) \quad \begin{aligned} & \mathcal{J}_{-h}(\underline{\mathbf{U}}_h, \mathbf{u}_h, p_h) = \\ & \| -(\nabla^t \underline{\mathbf{U}}_h)^t + \nabla p_h + \lambda \underline{\mathbf{U}}_h^t \mathbf{u}_h - \mathbf{f} \|_{-h}^2 + \|\nabla^t \mathbf{u}_h\|_0^2 + \|\underline{\mathbf{U}}_h - \nabla \mathbf{u}_h^t\|_0^2. \end{aligned}$$

We note that residuals of equations (2.9) and (2.10) can be added to (3.17) yielding an *augmented* negative norm functional given by

$$(3.18) \quad \begin{aligned} & \mathcal{J}_{-h}(\underline{\mathbf{U}}_h, \mathbf{u}_h, p_h) = \\ & \| -(\nabla^t \underline{\mathbf{U}}_h)^t + \nabla p_h + \lambda \underline{\mathbf{U}}_h^t \mathbf{u}_h - \mathbf{f} \|_{-h}^2 + \|\nabla^t \mathbf{u}_h\|_0^2 + \|\underline{\mathbf{U}}_h - \nabla \mathbf{u}_h^t\|_0^2 \\ & + \|\nabla(\text{tr} \underline{\mathbf{U}})\|_0^2 + \|\nabla \times \underline{\mathbf{U}}\|_0^2. \end{aligned}$$

This functional has not been analyzed in [3] and will not be discussed here.

Let \mathbf{X}^h denote a finite element subspace of \mathbf{X} , where \mathbf{X} is given by (3.2). Then the least-squares principle for (3.17) is:

seek $\mathcal{U}_h = (\underline{\mathbf{U}}_h, \mathbf{u}_h, p_h) \in \mathbf{X}^h$ such that

$$(3.19) \quad \mathcal{J}_{-h}(\underline{\mathbf{U}}_h, \mathbf{u}_h, p_h) \leq \mathcal{J}_{-h}(\underline{\mathbf{V}}_h, \mathbf{v}_h, q_h) \quad \forall \mathcal{V}_h = (\underline{\mathbf{V}}_h, \mathbf{v}_h, q_h) \in \mathbf{X}^h.$$

It is not difficult to see that the Euler-Lagrange equation for the principle (3.19) constitutes a variational problem of the form

seek $\mathcal{U}_h = (\underline{\mathbf{U}}_h, \mathbf{u}_h, p_h) \in \mathbf{X}^h$ such that

$$(3.20) \quad \mathcal{B}_{-h}(\mathcal{U}_h, \mathcal{V}_h) = 0 \quad \forall \mathcal{V}_h \in \mathbf{X}^h,$$

where

$$\begin{aligned} & \mathcal{B}_{-h}(\mathcal{U}_h, \mathcal{V}_h) = \\ & \left(-(\nabla^t \underline{\mathbf{U}}_h)^t + \nabla p_h + \lambda \underline{\mathbf{U}}_h^t \mathbf{u}_h - \mathbf{f}, -(\nabla^t \underline{\mathbf{V}}_h)^t + \nabla q_h + \lambda (\underline{\mathbf{U}}_h^t \mathbf{v}_h + \underline{\mathbf{V}}_h^t \mathbf{u}_h) \right)_{-h} \\ & + (\nabla^t \mathbf{u}_h, \nabla^t \mathbf{v}_h)_0 + (\underline{\mathbf{U}}_h - \nabla \mathbf{u}_h^t, \underline{\mathbf{V}}_h - \nabla \mathbf{v}_h^t)_0. \end{aligned}$$

Properties of approximations defined by (3.20) are summarized in the following theorem, proof of which can be found in [3].

THEOREM 3.1. *Assume that $\{(\lambda, (\underline{\mathbf{U}}(\lambda), \mathbf{u}(\lambda), p(\lambda))) \mid \lambda \in \Lambda\}$ is a regular branch of solutions of the Navier-Stokes equations, such that*

$$\Lambda \ni \lambda \mapsto \mathcal{U}(\lambda) = (\underline{\mathbf{U}}(\lambda), \mathbf{u}(\lambda), p(\lambda))$$

is a continuous map from Λ to $\mathbf{W} = \tilde{\mathbf{H}}^{-1}(\Omega) \times [\mathbf{H}^2(\Omega) \cap \mathbf{H}_0^1(\Omega)] \times [H^1(\Omega) \cap L_0^2(\Omega)]$. Assume also that for any $\mathcal{U} \in \mathbf{W}$, there exists $\mathcal{U}_h \in \mathbf{X}^h$ such that

$$\|\mathcal{U} - \mathcal{U}_h\|_{\mathbf{X}} \leq Ch\|\mathcal{U}\|_{\mathbf{W}}.$$

Then, there exist $\alpha > 0$, $h_1 > 0$ and $\tilde{\mathcal{U}}_h(\lambda) = (\tilde{\underline{\mathbf{U}}}_h(\lambda), \tilde{\mathbf{u}}_h(\lambda), \tilde{p}_h(\lambda)) \in C^0(\Lambda, \mathbf{X}^h)$ such that, for all $h \leq h_1$, $\{(\lambda, \tilde{\mathcal{U}}_h(\lambda)), \lambda \in \Lambda\}$ is a regular branch of solutions of (3.20) that is unique in the ball

$$\mathcal{S}_\alpha = \{\mathcal{V}_h \in \mathbf{X}^h \mid \|\mathcal{U}(\lambda) - \mathcal{V}_h\|_{\mathbf{X}} \leq \alpha\}, \quad \forall \lambda \in \Lambda.$$

Furthermore,

$$(3.21) \quad \begin{aligned} & \|\tilde{\underline{\mathbf{U}}}_h(\lambda) - \underline{\mathbf{U}}(\lambda)\|_0 + \|\tilde{\mathbf{u}}_h(\lambda) - \mathbf{u}(\lambda)\|_1 + \|\tilde{p}_h(\lambda) - p(\lambda)\|_0 \\ & \leq Ch(\|\underline{\mathbf{U}}(\lambda)\|_1 + \|\mathbf{u}(\lambda)\|_2 + \|p(\lambda)\|_1). \end{aligned}$$

4. Implementation. There are several issues that must be addressed in the algorithmic development of the negative norm least-squares method described in §3.1. First, one must choose a finite element space \mathbf{X}^h for the discretization of (3.20). Second, once \mathbf{X}^h is chosen, (3.20) yields a nonlinear algebraic system that must be solved in an iterative manner. Third, the use of norm (3.14) requires evaluation of the operator B^h . Lastly, the use of this norm also has impact on the design of solvers for the nonlinear algebraic system. In what follows we discuss these implementation issues starting with the choice of the discretization space \mathbf{X}^h .

Because the least-squares method is not subject to stability conditions, such as the inf-sup condition, the choice of \mathbf{X}^h is only guided by the desired approximation properties. In particular, here we employ the bilinear space Q_1 for the approximation of all variables, i.e.,

$$\mathbf{X}^h = [Q_1]^{n^2} \times [Q_1 \cap H_0^1(\Omega)]^n \times [Q_1 \cap L_0^2(\Omega)],$$

where n denotes the space dimension. We will use $\{\phi_h^i\}_{i=1}^N$ to denote a nodal basis of the finite element space Q_1 , and $\{\mathcal{V}_h^i\}_{i=1}^M$ to denote a nodal basis for the space \mathbf{X}^h . Although components of each \mathcal{V}_h^i can be expressed in terms of the nodal basis for Q_1 , we use the notation $\mathcal{V}_h^i = (\underline{\mathbf{v}}_h^i, \mathbf{v}_h^i, q_h^i)$ to distinguish the basis components for the different variables. For simplicity we agree to denote a finite element function $u_h \in Q_1$ and the set of nodal values of this function with the same symbol. Thus, depending on the context, $\mathcal{U}_h = (\underline{\mathbf{U}}_h, \mathbf{u}_h, p_h)$ will be identified either with a finite element function in \mathbf{X}^h , or with a block vector whose blocks are the coefficients of the individual functions in \mathcal{U}_h . We also recall the inequality

$$(4.1) \quad h^2 \frac{1}{C} \|u_h\|_{l_2}^2 \leq \int_{\Omega} [u_h(\mathbf{x})]^2 d\Omega \leq h^2 C \|u_h\|_{l_2}^2,$$

where $\|\cdot\|_{l_2}$ denotes the Euclidean norm in \mathbf{R}^n , that is valid for all $u_h \in Q_1$.

For the solution of the nonlinear system (3.20) we consider Newton's method. To define Newton's method, let us formally write this problem as

$$(4.2) \quad F_{-h}(\lambda, \mathcal{U}_h) = 0.$$

Let $\mathcal{U}_h^0 = (\underline{\mathbf{U}}_h^0, \mathbf{u}_h^0, p_h^0)$ denote an initial guess for Newton's method. Then, the sequence of Newton iterates $\mathcal{U}_h^k = (\underline{\mathbf{U}}_h^k, \mathbf{u}_h^k, p_h^k)$, $k \geq 1$, is generated recursively by solving the linear systems

$$(4.3) \quad D_{\mathcal{U}}F_{-h}(\lambda, \mathcal{U}_h^{k-1})\Delta\mathcal{U}_h^k = -F_{-h}(\lambda, \mathcal{U}_h^k),$$

and updating \mathcal{U}_h^{k-1} by $\Delta\mathcal{U}_h^k$:

$$\mathcal{U}_h^k = \mathcal{U}_h^{k-1} + \Delta\mathcal{U}_h^k.$$

If the hypotheses of Theorem 3.1 hold, then it is not difficult to see that Newton's method will have a nontrivial attraction ball, i.e., one can guarantee that the linear system (4.3) has a unique solution. Indeed, let us assume that $\{(\lambda, (\underline{\mathbf{U}}(\lambda), \mathbf{u}(\lambda), p(\lambda))) \mid \lambda \in \Lambda\}$ is a regular branch of solutions to (2.6)-(2.8), (2.3) that is being approximated by solving (3.20). Then, according to Theorem 3.1 the former problem will have a regular branch of discrete solutions $\{(\lambda, (\tilde{\underline{\mathbf{U}}}_h(\lambda), \tilde{\mathbf{u}}_h(\lambda), \tilde{p}_h(\lambda))) \mid \lambda \in \Lambda\}$ that is unique in the ball S_α . It follows then, that the Jacobian matrix $D_{\mathcal{U}}F_{-h}(\lambda, \cdot)$ is nonsingular in a nontrivial neighborhood of $\tilde{\mathcal{U}}_h(\lambda)$. As a result, the attraction ball of Newton's method is nontrivial and the matrix $D_{\mathcal{U}}F_{-h}(\lambda, \mathcal{U}_h^{k-1})$ is guaranteed to be nonsingular, provided that \mathcal{U}_h^{k-1} is close enough to $\tilde{\mathcal{U}}_h(\lambda)$. Moreover, since $D_{\mathcal{U}}F_{-h}(\lambda, \cdot)$ is exactly the Hessian of (3.5), it follows that the matrix $D_{\mathcal{U}}F_{-h}(\lambda, \mathcal{U}_h^{k-1})$ is necessarily symmetric and positive definite in a neighborhood of $\tilde{\mathcal{U}}_h(\lambda)$. Owing to the use of negative inner products this matrix is also dense. As a result, assembly of $D_{\mathcal{U}}F_{-h}(\lambda, \mathcal{U}_h^{k-1})$ is not feasible in practice, i.e., the system (4.3) must be solved by an assembly-free method. Consequently, symmetry and positive definiteness of $D_{\mathcal{U}}F_{-h}(\lambda, \mathcal{U}_h^{k-1})$ are essential for practical implementation of the negative norm method since they allow one to solve (4.3) by robust iterative methods. In particular, for the solution of (4.3) here we consider a preconditioned conjugate gradient method implemented without assembly of $D_{\mathcal{U}}F_{-h}(\lambda, \mathcal{U}_h^{k-1})$, even at the element level. The two critical steps at each iteration of this method are computation of the matrix-vector product of $D_{\mathcal{U}}F_{-h}(\lambda, \mathcal{U}_h^{k-1})$ and the conjugate direction vector, and computation of the action of the preconditioner. We discuss first evaluation of the matrix-vector product; the choice of the preconditioner and its application are considered later. To this end let \mathcal{U}_h and \mathcal{V}_h denote arbitrary functions in \mathbf{X}^h (resp. their coefficient vectors). Then

$$(4.4) \quad (\mathcal{V}_h)^t \cdot D_{\mathcal{U}}F_{-h}(\lambda, \mathcal{U}_h^{k-1}) \cdot \mathcal{U}_h = \mathcal{DB}_{-h}[\mathcal{U}_h^{k-1}](\mathcal{U}_h, \mathcal{V}_h),$$

where the bilinear form $\mathcal{DB}_{-h}[\mathcal{U}_h^{k-1}](\mathcal{U}_h, \mathcal{V}_h)$ is given by

$$(4.5) \quad \begin{aligned} & \mathcal{DB}_{-h}[\mathcal{U}_h^{k-1}](\mathcal{U}_h, \mathcal{V}_h) \\ &= \left(-(\nabla^t \underline{\mathbf{U}}_h^{k-1})^t + \nabla p_h^{k-1} + \lambda (\underline{\mathbf{U}}_h^{k-1})^t \mathbf{u}_h^{k-1} - \mathbf{f}, \right. \\ & \quad \left. \lambda (\underline{\mathbf{U}}_h^t \mathbf{v}_h + (\underline{\mathbf{V}}_h)^t \mathbf{u}_h) \right)_{-h} \\ &+ \left(-(\nabla^t \underline{\mathbf{U}}_h)^t + \nabla p_h + \lambda \left((\underline{\mathbf{U}}_h^{k-1})^t \mathbf{u}_h + \underline{\mathbf{U}}_h^t \mathbf{u}_h^{k-1} \right), \right. \\ & \quad \left. -(\nabla^t \underline{\mathbf{V}}_h)^t + \nabla q_h + \lambda \left((\underline{\mathbf{U}}_h^{k-1})^t \mathbf{v}_h + (\underline{\mathbf{V}}_h)^t \mathbf{u}_h^{k-1} \right) \right)_{-h} \\ &+ (\nabla^t \mathbf{u}_h, \nabla^t \mathbf{v}_h)_0 + (\underline{\mathbf{U}}_h - \nabla \mathbf{u}_h^t, \underline{\mathbf{V}}_h - \nabla (\mathbf{v}_h)^t)_0. \end{aligned}$$

As a result, components of the matrix-vector product $D_{\mathcal{U}}F_{-h}(\lambda, \mathcal{U}_h^{k-1}) \cdot \mathcal{U}_h$ can be computed according to the formula

$$[D_{\mathcal{U}}F_{-h}(\lambda, \mathcal{U}_h^{k-1}) \cdot \mathcal{U}_h]_i = \mathcal{DB}_{-h}[\mathcal{U}_h^{k-1}](\mathcal{U}_h, \mathcal{V}_h^i), \quad i = 1, \dots, M.$$

In order to evaluate (4.5) it is necessary to compute several discrete negative inner products $(\cdot, \cdot)_{-h}$. These inner products are computed according to (3.15), i.e., this process involves application of the operator B^h . Recall that B^h must be spectrally equivalent to S^h . This can be accomplished by choosing B^h to be a preconditioner for S^h ; see [7]. Although in most cases B^h can be identified with a suitable symmetric matrix, here we prefer to consider B^h as a black-box type algorithm for the Poisson equation. For example, B^h can be defined in terms of several multigrid V-cycles for (3.9), see [7], or more generally, by any approximation scheme for this problem. With these assumptions evaluation of, e.g., the first term in (4.5) can be accomplished as follows. First, using (3.15), we have that

$$\begin{aligned}
 & \left(-(\nabla^t \underline{\mathbf{U}}_h^{k-1})^t + \nabla p_h^{k-1} + \lambda(\underline{\mathbf{U}}_h^{k-1})^t \mathbf{u}_h^{k-1} - \mathbf{f}, \lambda(\underline{\mathbf{U}}_h^t \mathbf{v}_h^i + (\underline{\mathbf{V}}_h^i)^t \mathbf{u}_h) \right)_{-h} \\
 &= \left((\alpha h^2 I + B^h) \left(-(\nabla^t \underline{\mathbf{U}}_h^{k-1})^t + \nabla p_h^{k-1} + \lambda(\underline{\mathbf{U}}_h^{k-1})^t \mathbf{u}_h^{k-1} - \mathbf{f} \right), \right. \\
 & \quad \left. \lambda(\underline{\mathbf{U}}_h^t \mathbf{v}_h^i + (\underline{\mathbf{V}}_h^i)^t \mathbf{u}_h) \right)_0 \\
 &= \alpha h^2 \left(-(\nabla^t \underline{\mathbf{U}}_h^{k-1})^t + \nabla p_h^{k-1} + \lambda(\underline{\mathbf{U}}_h^{k-1})^t \mathbf{u}_h^{k-1} - \mathbf{f}, \lambda(\underline{\mathbf{U}}_h^t \mathbf{v}_h^i + (\underline{\mathbf{V}}_h^i)^t \mathbf{u}_h) \right)_0 \\
 & \quad + \left(B^h \mathbf{g}, \lambda(\underline{\mathbf{U}}_h^t \mathbf{v}_h^i + (\underline{\mathbf{V}}_h^i)^t \mathbf{u}_h) \right)_0,
 \end{aligned}$$

where

$$\mathbf{g} = -(\nabla^t \underline{\mathbf{U}}_h^{k-1})^t + \nabla p_h^{k-1} + \lambda(\underline{\mathbf{U}}_h^{k-1})^t \mathbf{u}_h^{k-1} - \mathbf{f}.$$

All terms involving αh^2 are essentially weighted L^2 -inner products which can be computed in a standard manner. To compute the remaining terms B^h must be applied to \mathbf{g} . For this purpose we consider \mathbf{g} as a source term for (3.9) and form the vectors

$$(\mathbf{g}_1, \phi_h^i)_0 \quad \text{and} \quad (\mathbf{g}_2, \phi_h^i)_0, \quad i = 1, \dots, N.$$

where $\{\phi_h^i\}_{i=1}^N$ is a nodal basis for $Q_1 \cap H_0^1(\Omega)$. These vectors are the data for the black-box evaluator of B^h which returns the nodal coefficients of a finite element function \mathbf{g}_h representing $B^h \mathbf{g}$. Thus,

$$\left(B^h \mathbf{g}, \lambda(\underline{\mathbf{U}}_h^t \mathbf{v}_h^i + (\underline{\mathbf{V}}_h^i)^t \mathbf{u}_h) \right)_0 = \left(\mathbf{g}_h, \lambda(\underline{\mathbf{U}}_h^t \mathbf{v}_h^i + (\underline{\mathbf{V}}_h^i)^t \mathbf{u}_h) \right)_0.$$

The right-hand side above is an L^2 inner product which can now be computed in a standard manner. Evaluation of all other terms involving B^h is identical.

Let us now discuss the choice of a preconditioner for the conjugate gradient method. Here we follow an approach suggested in [7]. Recall that, as a consequence of Theorem 3.1, the form $\mathcal{DB}_{-h}[\mathcal{U}_h^{k-1}](\cdot, \cdot)$ is coercive and continuous on \mathbf{X}^h , provided that \mathcal{U}_h^{k-1} is sufficiently close to a nonsingular solution of the Navier-Stokes equations. As a result,

$$\begin{aligned}
 (4.6) \quad \frac{1}{C} \left(\|\underline{\mathbf{V}}_h\|_0^2 + \|\mathbf{v}_h\|_1^2 + \|p_h\|_0^2 \right) &\leq \mathcal{DB}_{-h}[\mathcal{U}_h^{k-1}](\mathcal{V}_h, \mathcal{V}_h) \\
 &\leq C \left(\|\underline{\mathbf{V}}_h\|_0^2 + \|\mathbf{v}_h\|_1^2 + \|p_h\|_0^2 \right)
 \end{aligned}$$

for all $\mathcal{V}_h \in \mathbf{X}^h$. Let G and D denote matrices with entries given by $G_{ij} = (\phi_h^i, \phi_h^j)_0$ and $D_{ij} = (\nabla \phi_h^i, \nabla \phi_h^j)_0$, respectively. We introduce a block diagonal matrix G_{n^2} with n^2 blocks given by G , and a block diagonal matrix D_n with n blocks given by D . Consider then the

block matrix

$$A = \begin{pmatrix} G_{n^2} & 0 & 0 \\ 0 & D_n & 0 \\ 0 & 0 & G \end{pmatrix}.$$

From (4.4) it follows that

$$(\mathcal{V}_h)^t \cdot D_{\mathcal{U}} F_{-h}(\lambda, \mathcal{U}_h^{k-1}) \cdot \mathcal{V}_h = \mathcal{DB}_{-h}[\mathcal{U}_h^{k-1}](\mathcal{V}_h, \mathcal{V}_h).$$

Combined with (4.6) this identity yields the bounds

$$\frac{1}{C}(\mathcal{V}_h)^t \cdot A \cdot \mathcal{V}_h \leq (\mathcal{V}_h)^t \cdot D_{\mathcal{U}} F_{-h}(\lambda, \mathcal{U}_h^{k-1}) \cdot \mathcal{V}_h \leq C(\mathcal{V}_h)^t \cdot A \cdot \mathcal{V}_h,$$

i.e., the matrix A is spectrally equivalent to $D_{\mathcal{U}} F_{-h}(\lambda, \mathcal{U}_h^{k-1})$. To define the preconditioner for the conjugate gradient method note that (4.1) implies spectral equivalence of G and the matrix $h^2 I$. Definitions of D and B^h also imply that $\tilde{D} = B^{h-1}$ is spectrally equivalent to D . As a result, the matrix

$$(4.7) \quad \tilde{A} = \begin{pmatrix} h^2 I_{n^2} & 0 & 0 \\ 0 & \tilde{D}_n & 0 \\ 0 & 0 & h^2 I \end{pmatrix}.$$

is spectrally equivalent to $D_{\mathcal{U}} F_{-h}(\lambda, \mathcal{U}_h^{k-1})$, and can be used to precondition the conjugate gradient method. To apply this preconditioner we need again the black-box algorithm for B^h . Indeed, given a vector $\mathcal{V}_h = (\underline{\mathbf{V}}_h, \mathbf{v}_h, q_h)$, application of \tilde{A} to \mathcal{V}_h involves solution of (3.9) with the velocity component \mathbf{v}_h serving as a source term. Thus, we first form the data vectors

$$\mathbf{g}_1 = (\mathbf{v}_h^1, \phi_h^i)_0 \quad \text{and} \quad \mathbf{g}_2 = (\mathbf{v}_h^1, \phi_h^i)_0, \quad i = 1, \dots, N$$

and then apply the algorithm for B^h .

5. Numerical results. In this section we report numerical experiments with the negative norm least-squares method implemented as outlined in §4. For all experiments we take Ω to be the unit square. We consider two examples of planar flows. The first example is an artificial planar flow, that is we begin with a known smooth velocity and pressure fields and then compute the data by evaluating the first-order system (2.6)-(2.8) at these fields. Results for this example are presented in §5.1. The second example involves the fictitious lid driven cavity (or driven cavity) flow. This flow is a popular test example which is well-documented in many benchmark studies; see, e.g., [11], [15]-[18]. Results for this example are given in §5.2. Lastly, in §5.3 the negative norm method is compared with two other least-squares methods for the velocity-flux equations based on the L^2 -functionals (3.1) and (3.6), respectively.

5.1. Numerical results: smooth solution. For all examples in this section we consider an exact solution given by

$$(5.1) \quad \begin{aligned} \mathbf{u} &= (\exp(x) \cos(y) + \sin(y), -\exp(x) \sin(x) + (1 - x^3))^t, \\ \underline{\mathbf{U}} &= \nabla \mathbf{u}^t, \\ p &= \sin(y) \cos(x) + xy^2 - \frac{1}{6} - \sin(1)(1 - \cos(1)). \end{aligned}$$

TABLE 5.1

Convergence rates of the negative norm method for $\alpha = 0.2$ and varying tolerances in the computation of B^h

Δ^{-1} tolerance	10^{-1}	10^{-2}	10^{-3}	10^{-4}	10^{-5}	BA
Variable	L^2 -error rate					
\mathbf{u}	-0.614	0.370	1.861	1.869	1.869	-
$\underline{\mathbf{U}}$	-0.717	-0.052	1.535	1.586	1.587	1.000
p	-1.261	-0.066	1.559	1.580	1.584	1.000
Variable	H^1 -error rate					
\mathbf{u}	-0.632	0.791	1.014	1.016	1.016	1.000
$\underline{\mathbf{U}}$	-1.110	-0.349	0.652	0.665	0.666	-
p	-1.439	-0.622	0.677	0.707	0.708	-

TABLE 5.2

Convergence rates of the negative norm method with a fixed tolerance for B^h and varying α

Error	L^2 -error rate				H^1 -error rate				
	α	0	0.2	1	BA	0	0.2	1	BA
\mathbf{u}	1.850	1.869	1.873	-	1.018	1.016	1.015	1.000	-
$\underline{\mathbf{U}}$	1.559	1.587	1.605	1.000	0.585	0.666	0.701	-	-
p	1.219	1.584	1.584	1.000	0.134	0.708	0.686	-	-

Since this exact solution is a fictitious flow which does not depend on Re , all computations are carried with $Re = 1$. Owing to the use of Q_1 elements in the implementation, the expected asymptotic rate of convergence for the negative norm method is $O(h)$, i.e., for h small enough we expect that

$$(5.2) \quad \|\underline{\mathbf{U}} - \underline{\mathbf{U}}_h\|_0 + \|\mathbf{u} - \mathbf{u}_h\|_1 + \|p - p_h\|_0 \leq Ch.$$

Note that in (5.2) the $O(h)$ convergence rate for the velocity approximation is asserted in the norm of $H^1(\Omega)$, whereas for the velocity flux and the pressure variables this rate is asserted in the norm of $L^2(\Omega)$. As a result, (5.2) is optimal when the velocity flux and the pressure are approximated by finite element spaces of one degree less than the spaces used for the velocity approximation. Here, we have chosen Q_1 elements for all variables solely for simplicity of the implementation.

Our first goal is to investigate how the choice of B^h and α in (3.14) affects validity of (5.2). Theoretically, this estimate should hold as long as the operator B^h remains spectrally equivalent to S^h (condition (3.12)), and α is positive (otherwise (3.14) reduces to the seminorm (3.13)). To assess the importance of (3.12) we fix $\alpha = 0.2$ and compute numerical rates of convergence for varying operators B^h . (This choice of α will become evident below.) For this purpose, B^h is evaluated using an iterative Poisson solver defined on the space $Q_1 \cap H_0^1(\Omega)$. The different choices for B^h are obtained by varying the relative tolerance for this solver. A large tolerance corresponds to an operator B^h that does not satisfy (3.12) well, whereas tighter tolerances yield operators B^h that are spectrally equivalent to S^h . Next, we consider how (5.2) is affected by the choice of α . For this purpose the tolerance of the Poisson solver for B^h is fixed equal to 10^{-5} , and computations are carried with $\alpha = 0$ and $\alpha = 1$. For all cases, convergence rates are estimated by computing approximate solutions on uniform grids with 17×17 and 33×33 grid lines respectively. Corresponding results are summarized in Tables 5.1-5.2. These tables contain results for both the rates asserted by estimate (5.2), as well as for rates that are not included in this estimate. The former are given in bold face symbols, with the column BA containing the expected rates (5.2). From the data in Table 5.1 we can conclude that the spectral equivalence condition (3.12) is critical for the

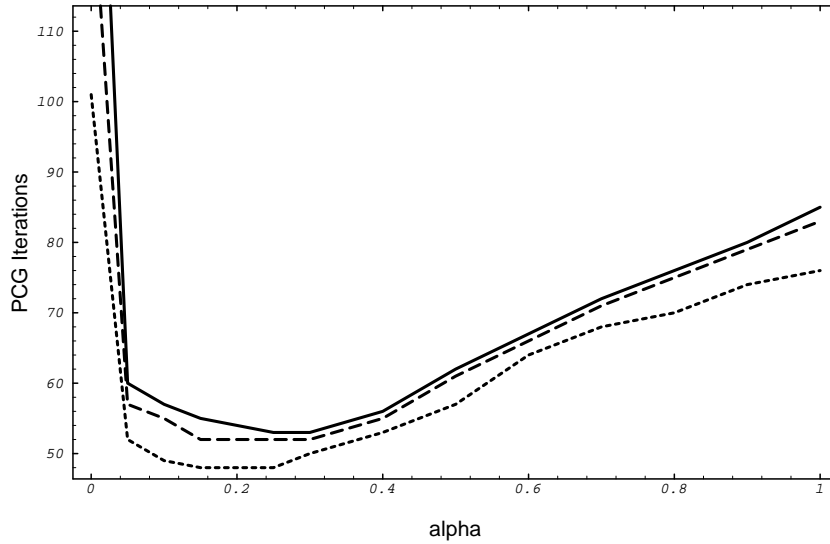


FIG. 5.1. Dependence of preconditioned conjugate gradient iterations on α

performance of the negative norm method. The first two columns in this table demonstrate a complete loss of convergence when B^h fails to satisfy (3.12), whereas the last three columns show that once B^h becomes spectrally equivalent to S^h , then approximations converge according to (5.2). We note that the individual L^2 -rates for $\underline{\mathbf{U}}$ and p are better than $O(h)$ which, most likely, is caused by the use of equal order approximation spaces for all variables. Table 5.2, on the other hand, suggests that the choice of α is less important for the validity of asymptotic convergence rates in (5.2). When $\alpha = 0$, the only significant drop occurs in the asymptotic rate for the H^1 -norm error of the pressure. However, this error is not included in (5.2) and, as a result, the total error $\|\underline{\mathbf{U}} - \underline{\mathbf{U}}_h\|_0 + \|\mathbf{u} - \mathbf{u}_h\|_1 + \|p - p_h\|_0$ still converges at a rate of $O(h)$.

Next we consider the importance of B^h and α for the overall performance of the preconditioned conjugate gradient method used to solve the discrete equations. Since α appears in the definition of the negative norm (3.14) its choice affects the properties of the algebraic system corresponding to the discrete variational problem. B^h , on the other hand, appears in both the negative norm (3.14) and the preconditioner (4.7). However, here we are only interested in the effect of B^h upon the preconditioner. Thus, in what follows we assume that B^h in (3.14) is fixed and use B_p^h to denote the operator employed in (4.7).

To determine the importance of α for the conjugate gradient method we fix the tolerances for B^h and B_p^h equal to 10^{-5} . Then we compare the number of preconditioned conjugate gradient iterations needed to achieve the same relative error tolerance in the solution of the linear system for values of α between 0 and 1. Corresponding results for 9×9 , 17×17 and 33×33 uniform grids are summarized in Figure 5.1. From these plots we can conclude that unless $\alpha > 0$, performance of the conjugate gradient method degrades significantly. Indeed, for all three grids $\alpha = 0$ results in the highest number of iterations (101, 133 and 174, respectively), while taking even a small positive α , e.g., $\alpha = 0.05$ helps to reduce the number of iterations more than twice. Even more importantly, when $\alpha = 0$ we see that the number of iterations grows as the number of grid lines increases, i.e., convergence of the conjugate gradient method is not independent of h . This behavior can be explained by noting that

TABLE 5.3
Number of conjugate gradient iterations with different preconditioners; $\alpha = 0.2$ and 10^{-5} tolerance for B^h

Preconditioner	Grid size			
	5x5	9x9	17x17	33x33
none	122	220	419	759
Jacobi	37	52	102	185
(4.7)	44	48	52	53

TABLE 5.4
Number of preconditioned conjugate gradient iterations for different choices of B_p^h

Grid	Δ^{-1} tolerance				
	0.5	0.1	0.001	0.0001	0.00001
9×9	137	49	48	48	48
17×17	258	56	52	52	52

setting $\alpha = 0$ in (3.17) yields a least-squares functional defined using the seminorm (3.13) for which the lower bound in (3.16) does not hold. From Fig. 5.1 it also appears that $\alpha > 0.2$ is sufficient to assure convergence of the conjugate gradient method which is virtually independent of h , with the fastest convergence occurring in the range $0.25 \leq \alpha \leq 0.30$. Thus, one can infer the existence of an optimal value for α . This value appears to depend mildly on the grid parameter h , e.g., for 9×9 grids it is given by $\alpha \approx 0.2$ whereas for 33×33 grids it is given by $\alpha \approx 0.3$. The ability of (4.7) to provide convergence independent of h for these values of α is also illustrated by the data in Table 5.3. This table compares the number of conjugate gradient iterations without preconditioning, using a Jacobi preconditioner, and using (4.7).

Lastly, to determine how the choice of B_p^h affects the preconditioner we fix $\alpha = 0.2$ and vary the tolerance in the Poisson solver used to compute B^h . Corresponding results are summarized in Table 5.4. The data in this table suggests that preconditioner (4.7) is not very sensitive with respect to the quality of B_p^h and that the overall performance of the conjugate gradient method depends more critically on α .

5.2. Numerical results: driven cavity flow. The two-dimensional lid driven cavity flow is often used to test numerical solvers for the Navier-Stokes equations. Although this example represents a fictitious flow it is well-documented in the literature and there is an abundance of benchmark results available for comparison. We recall that for the driven cavity flow $\mathbf{f} = \mathbf{0}$ and that the velocity boundary condition is given by $\mathbf{u} = (1, 0)$ on the top surface of the unit square and zero otherwise. For this example we have considered a Reynolds number of 100 and bilinear spaces defined on uniform triangulations of 17×17 , 33×33 , and 45×45 finite elements. Our numerical results are presented in Figures 5.2-5.3. Figure 5.2 contains directional plot of the velocity field and a contour plot of the vorticity, computed using 33×33 finite elements. For the second plot vorticity has been obtained using the computed velocity flux variable, i.e., $\omega = \underline{\mathbf{U}}_{21}^h - \underline{\mathbf{U}}_{12}^h$. Plots in Fig. 5.2 appear to be in a good agreement with similar plots reported in, e.g., [11]. Although the “eyeball” norm comparison with [11] is satisfactory, in Figure 5.3 we present a more quantitative measure for the performance of the least-squares method. In this figure velocity profiles through the geometrical center of the cavity are compared with the benchmark results of [11] computed using a finite difference scheme with 129×129 nodes. The first component of the velocity, denoted by u , is plotted along the vertical line $x = 0.5$, whereas the second component, denoted by v , is plotted along the horizontal line $y = 0.5$. We see that the u -velocity is very close to the benchmark data even for the coarse 17×17 grid, whereas matching the benchmark v -velocity is problematic for

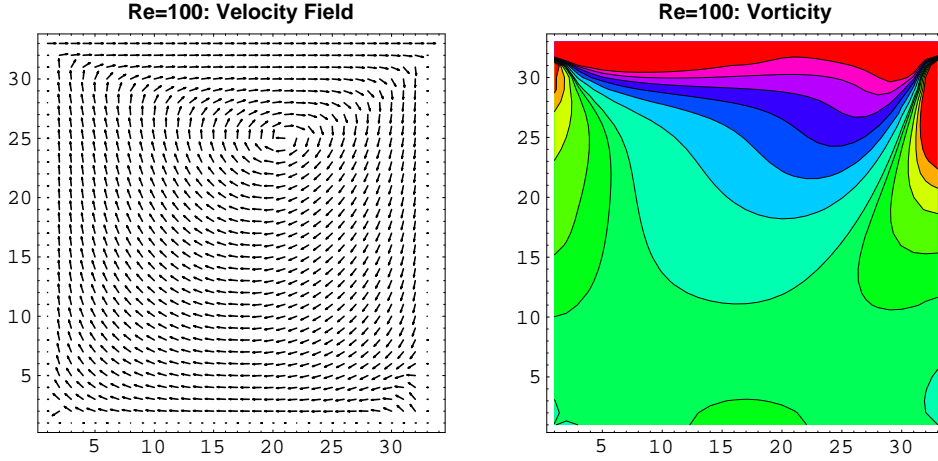


FIG. 5.2. Driven Cavity flow at $Re=100$: velocity field and vorticity contours

this grid size. However, increasing the grid size to 33×33 and then to 45×45 yields significant improvement in the v -velocity profile.

In §5.1 we saw that choosing $\alpha = 0$ leads to reduced H^1 -rates for the pressure approximation. In the present setting we found that the most affected variable is again the pressure. Specifically, $\alpha = 0$ leads to highly oscillatory pressure approximations. On the other hand, even a small positive α is sufficient to eliminate the oscillations. These observations are illustrated in Fig. 5.4 which shows contour lines of pressure approximations computed with $\alpha = 0$ and $\alpha = 0.01$.

5.3. Comparison with L^2 velocity flux methods. In this section we compare the negative norm method with the two L^2 least-squares methods based on (3.1) and (3.6), respectively. For all three methods we consider implementation using Q_1 finite element spaces. As a result, for smooth solutions, the asymptotic rate of convergence for the negative norm method is given again by (5.2), whereas for the augmented L^2 method (3.6) the corresponding estimate reads

$$(5.3) \quad \|\underline{\mathbf{U}} - \underline{\mathbf{U}}^h\|_1 + \|\mathbf{u} - \mathbf{u}^h\|_1 + \|p - p^h\|_1 \leq Ch;$$

see [2]. Since functional (3.1) is not norm-equivalent, no theoretical error estimates are available for this least-squares method. Note that in contrast to (5.2), estimate (5.3) asserts optimal convergence in the norm of H^1 for *all variables*. We recall that this is a consequence of the H^1 -norm equivalence of (3.6). Therefore, a fair comparison between (3.17) and (3.6) is hardly possible. For example, (5.3) is optimal when all unknowns are approximated by equal order finite element spaces, as is the case here, whereas (5.2) is optimal when the velocity field is approximated by spaces of one degree higher than used for $\underline{\mathbf{U}}$ and p . Similarly, (5.2) is valid as long as $\underline{\mathbf{U}} \in \tilde{\mathbf{H}}^1(\Omega)$, $p \in H^1(\Omega)$ and $\mathbf{u} \in \mathbf{H}^2(\Omega)$, whereas (5.3) requires all components to be at least in $H^2(\Omega)$. Thus, results of this section should not be viewed as a direct juxtaposition of the two methods but rather as a suggestion for the most appropriate scope of each method.

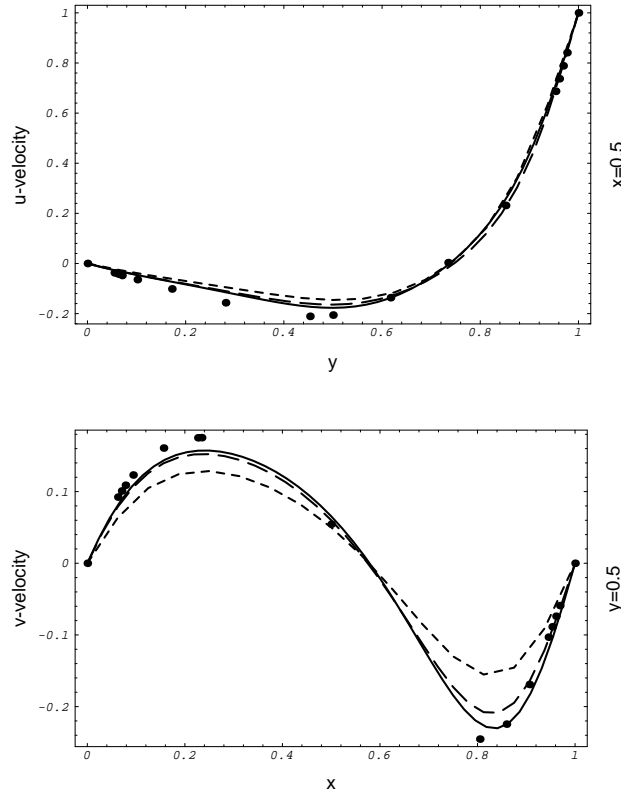


FIG. 5.3. Velocity profiles: negative norm least-squares for 17x17 (short dashes), 33x33 (long dashes) and 45x45 (solid line) bilinear elements vs. benchmark results of [11] (dots)

TABLE 5.5
Convergence rates for the H^{-1} method and L^2 least-squares methods (3.6) and (3.1).

Method	L^2 error rates			H^1 error rates		
	negative	(3.6)	(3.1)	negative	(3.6)	(3.1)
u	1.869	1.921	0.944	1.016	1.002	0.918
U	1.587	1.776	0.881	0.666	1.091	0.594
p	1.584	1.741	0.706	0.708	1.530	0.531

5.3.1. Smooth solutions. For the negative norm method we consider the rates obtained when $\alpha = 0.2$ and the tolerance for B^h is set to 10^{-5} ; see Table 5.1. Asymptotic convergence rates for the L^2 -methods are estimated using approximate solutions computed on a pair of uniform grids with 17x17 and 33x33 grid lines, respectively. Corresponding results are summarized in Table 5.4. Like in Tables 5.1-5.2, bold face in this table is used to denote asymptotic rates for the error components which are included in (5.2) and (5.3). The asymptotic rates of (3.6) in Table 5.5 are in excellent agreement with (5.3) and are higher than the H^1 -norm rates of the negative norm method. There is less difference in the L^2 -norm rates of these methods, but the augmented L^2 -method still has better convergence. In contrast, the

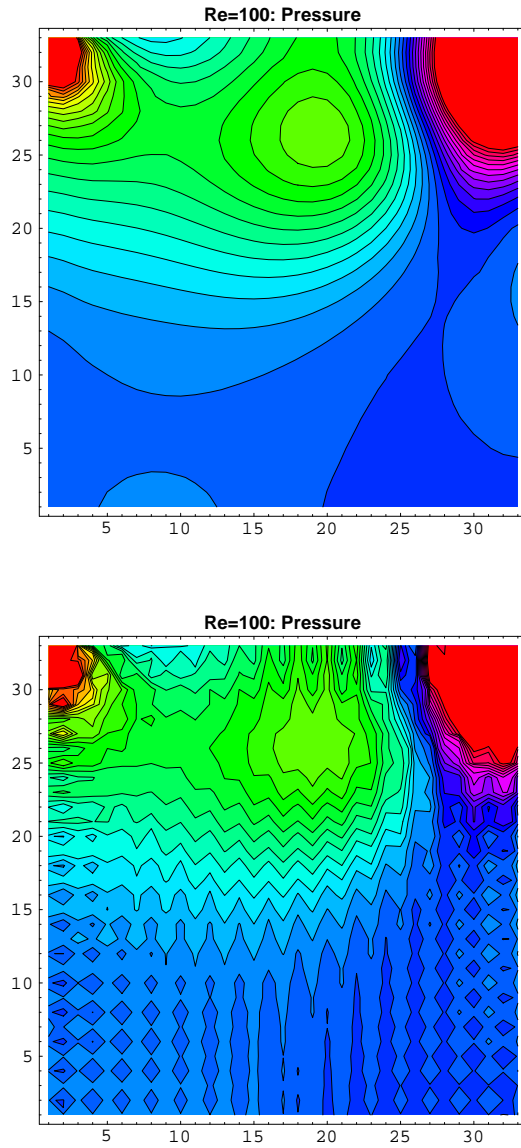


FIG. 5.4. Pressure contours for $Re = 100$ and 33×33 elements. $\alpha = 0.01$ (top) and $\alpha = 0$ (bottom)

method (3.1) consistently yields suboptimal convergence rates. In the L^2 -norm of the error these rates are of approximately one order less than the rates for (3.6). In the H^1 -norm of the error (3.1) converges at half the rate of (3.6). Although the H^1 -norm rates for (3.1) are closer to the rates of the negative norm method, in the L^2 -norm the former converges twice as fast as (3.1).

The data in Table 5.5 leads to the unambiguous conclusion that for smooth solutions the augmented L^2 -method ranks first, while the method (3.1) offers the worst performance. The main cause for this dismal performance of (3.1) is in the lack of norm-equivalence of the underlying least-squares functional. These results are consistent with numerical experiments

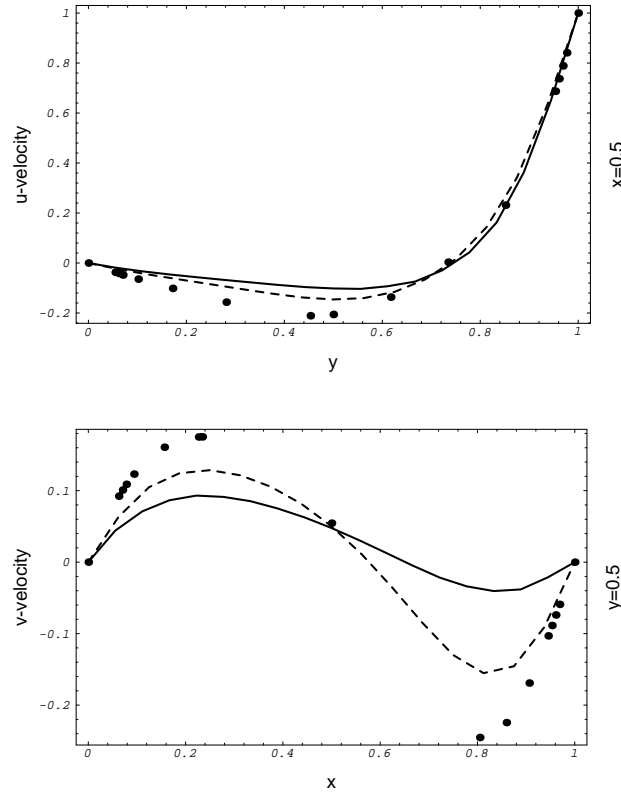


FIG. 5.5. Velocity profiles for the Driven Cavity flow: negative norm method (dashed lines) vs. the L^2 method (3.6) (solid lines).

performed using other non-norm equivalent functionals, where suboptimal convergence rates were also observed; see [6].

From the data in Table 5.5 we can conclude that, although performance of the negative norm method is not dramatically inferior to that of (3.6), the less complicated and straightforward implementation of the L^2 -method makes it more convenient when the exact solution is smooth enough. As we shall see in the next section, the real advantage of the negative norm method is revealed when solutions of the Navier-Stokes equations are not sufficiently regular.

5.3.2. Driven cavity flow. Discontinuity of the boundary data in the driven cavity flow leads to velocity fields that are not sufficiently regular for the least-squares method (3.6). Indeed, analysis of this method requires that minimization is carried over the space

$$\mathbf{X} = \{(\underline{\mathbf{U}}, \mathbf{u}, p) \in \tilde{\mathbf{H}}^1(\Omega) \times \mathbf{H}_0^1(\Omega) \times H^1(\Omega) \cap L_0^2(\Omega) \mid \mathbf{u} = \mathbf{0}, \mathbf{n} \times \underline{\mathbf{U}} = \underline{\mathbf{0}} \text{ on } \Gamma\};$$

see [2]. In view of the definition (2.5) it follows that components of the velocity field should be at least in $H^2(\Omega)$, which is not the case with the driven cavity flow. The lack of regu-

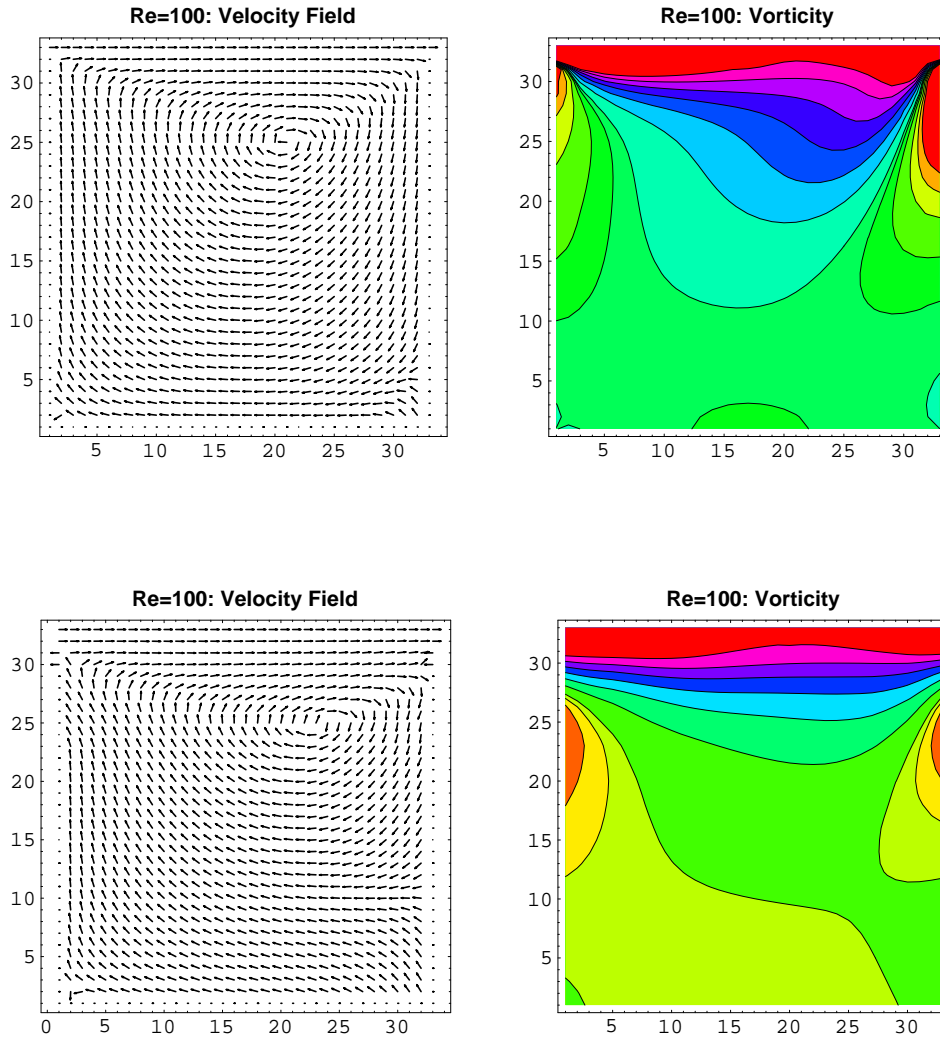


FIG. 5.6. Driven cavity flow at $Re=100$: negative norm method vs. the L^2 -method (3.6).

larity in the solution leads to poor performance of the method (3.6) for this problem. This can be seen from the plots presented in Fig. 5.5. Here we compare velocity profiles through the center of the cavity computed by (3.6) (solid lines) and the negative norm method (3.17) (dashed lines), with the benchmark results of [11], using 17×17 bilinear elements. Although (3.6) yields reasonable approximation for the u -velocity, it significantly underestimates the v -velocity component. These results suggest that the negative norm method has an advantage over the L^2 -method for problems with less regular solutions. Similar conclusions can be drawn from the results presented in Fig. 5.6. This figure contains velocity fields and vorticity contours computed by the negative norm method (3.17) and the L^2 -method (3.6) using 33×33 bilinear elements. Plots in Fig. 6.6 clearly indicate a qualitative difference between

these two methods, moreover, approximations computed by (3.6) do not compare well with the benchmark [11].

Acknowledgments. I wish to thank Prof. T. Manteuffel for the careful reading of this manuscript and the numerous suggestions which helped to improve it significantly.

REFERENCES

- [1] P.B. BOCHEV, *Analysis of least-squares finite element methods for the Navier-Stokes equations*, SIAM J. Num. Anal., 34 (1997), to appear.
- [2] P. BOCHEV, Z. CAI, T.A. MANTEUFFEL AND S. F. MCCORMICK, *Analysis of velocity-flux least-squares principles for the Navier-Stokes equations: Part I*, SIAM J. Num. Anal. to appear.
- [3] P. BOCHEV, T.A. MANTEUFFEL AND S. F. MCCORMICK, *Analysis of velocity-flux least-squares principles for the Navier-Stokes equations: Part II*, submitted.
- [4] P. BOCHEV AND M. GUNZBURGER, *A least-squares finite element method for the Navier-Stokes equations*, Appl. Math. Lett., 6/2 (1993), pp. 27–30.
- [5] ———, *Accuracy of least-squares methods for the Navier-Stokes equations*, Comput. & Fluids, 22 (1993), pp. 549–563.
- [6] ———, *Analysis of least-squares finite element methods for the Stokes equations*, Math. Comp., 63 (1994), pp. 479–506.
- [7] J. H. BRAMBLE, R. D. LAZAROV, AND J. E. PASCIAK, *A least-squares approach based on a discrete minus one inner product for first order systems*, Technical report 94-32 (1994), Mathematical Science Institute, Cornell University, 23 pages.
- [8] Z. CAI, T. MANTEUFFEL, AND S. MCCORMICK, *First-order system least-squares for velocity-vorticity-pressure form of the Stokes equations, with application to linear elasticity*, Electron. Trans. Numer. Anal., 3 (1995), pp.150–159.
- [9] Z. CAI, T.A. MANTEUFFEL AND S. F. MCCORMICK, *First-order system least squares for the Stokes equations, with application to linear elasticity*, SIAM J. Num. Anal., to appear.
- [10] P. G. CIARLET, *The finite element method for elliptic problems*, North-Holland, Amsterdam, 1978.
- [11] U. GHIA, K. N. GHIA, AND C. T. SHIN, *High-Re solutions for incompressible flow using the Navier-Stokes equations and a multigrid method*, J. Comput. Phys., 48 (1982), pp. 387–411.
- [12] V. GIRAULT AND P. RAVIART, *Finite Element Methods for Navier-Stokes Equations*, Springer, Berlin, 1986.
- [13] R. GLOWINSKI, B. MANTEL, J. PERIAUX, P. PERRIER AND O. PIRONNEAU, *On an efficient new preconditioned conjugate gradient method. Application to the in-core solution of the Navier-Stokes equations via non-linear least-squares and finite element methods*, in Finite Elements in Fluids, Volume 4, R. H. Gallagher, ed., Willey, 1982, pp. 365–401.
- [14] M. GUNZBURGER, *Finite Element Methods for Viscous Incompressible Flows*, Academic, Boston, 1989.
- [15] B. JIANG, T. LIN, AND L. POVINELLI, *A least-squares finite element method for 3D incompressible Navier-Stokes equations*, AIAA Report 93-0338, AIAA, New York, 1993.
- [16] B.-N. JIANG, T. LIN, AND L. POVINELLI, *Large-scale computation of incompressible viscous flow by least-squares finite element method*, Comput. Methods Appl. Mech. Engrg., 114 (1994), pp. 213–231.
- [17] D. LEFEBVRE, J. PERAIRE, AND K. MORGAN, *Least-squares finite element solution of compressible and incompressible flows*, Internat. J. Numer. Methods. Heat Fluid Flow, 2 (1992), pp. 99–113.
- [18] L. TANG, T. CHENG AND T. TSANG, *Transient solutions for three-dimensional lid-driven cavity flows by a least-squares finite element method*, Internat. J. Numer. Methods Fluids, 21 (1995), pp. 413–432.